32nd URSI GASS, Montreal, 19–26 August 2017

Channel Estimation Algorithms and Their Impact on Wideband Millimeter Wave Channel Characteristics

Wei Fan(1), Yilin Ji(1), Fengchun Zhang(1), and Gert F. Pedersen(1)
(1) Department of Electronic Systems, Aalborg University, 9000, Aalborg, Denmark

Abstract

The demand for higher data rate has motivated research in millimeter wave (mm-Wave) bands for 5G cellular systems. Accurate channel characterization at mm-Wave bands has gained significant interest in recent years, since it is important for system design and performance evaluation of future communication systems. In this paper, a mm-Wave channel sounding campaign based on a rotational horn and a virtual uniform circular array (UCA) was performed in a line-of-sight (LOS) and obstructed-LOS scenario in an indoor environment. Three channel estimation algorithms were implemented for the UCA data and compared with the horn antenna measurement results. The channel characteristics, e.g. mean angle of arrival, angle spread, mean delay and delay spread were analyzed for different algorithms. The measured results demonstrated the impact of channel estimation algorithms in radio channel parameters.

1 Introduction

5G is moving towards frequency bands above 6 GHz, since frequencies in the legacy bands are congested and mostly occupied. Huge unlicensed frequency bandwidths are available at mm-Wave bands. Further, we have the possibility to implement massive antenna arrays both at the mobile and base station due to small wavelength at mm-Wave bands. Accurate channel characterization is important for future mm-Wave system design and performance evaluation [1, 2, 3]. So far, high gain directional antennas have been extensively used in mm-Wave channel measurement [2]. High gain directional antennas are attractive since it offers better link budget and they are cost effective. The channel spatial characteristics can be simply obtained via rotating the directional antennas. However, mechanical steering of directive antennas is slow for channel sounding and the beam-width of the antenna is typically limited. Mm-Wave channel sounders equipped with a massive number of antenna elements and respective RF transceiver chains are not popular, due to the high cost.

Another widely utilized measurement system is so-called virtual array systems, where one antenna element is mechanically repositioned at predefined locations to form a two dimension (2D) or 3D virtual antenna array [4, 1]. Only one antenna and one associated radio frequency (RF) transceiver chain are needed at the transmitter (Tx) and receiver (Rx) side, respectively. This system has been utilized both for indoor and outdoor channel sounding measurements. The measurement system is attractive and widely adopted, due to its simplicity, low cost and flexibility. However, it can only be applied in static environments, since it is assumed that channel profiles remain static for all element locations (i.e. antenna elements in the virtual array).

In this paper, mm-Wave channel sounding based on a rotational horn and a virtual uniform circular array (UCA) was performed in a LOS and obstructed-LOS scenario. Different channel estimation algorithms, e.g. Classical beamforming [4, 5], frequency invariant beamforming [6], maximum likelihood (ML) [7] estimator were developed to analyze the data in the virtual array and compared with rotational horn measured results. The channel characteristics, e.g. mean angle of arrival, angle spread, mean delay and delay spread were analyzed based on the obtained power-angle-delay profiles with different algorithms.

2 Measurement campaign

2.1 VNA based channel sounding system

An illustration of the measurement setup is shown in Fig. 1, where the system consists of a two-port VNA, a Tx antenna and a Rx antenna. A vertically polarizied wideband Biconical antenna was utilized as the Tx antenna, while two types of antennas were selected for the Rx antenna. With the two different Rx antennas, two sets of measurements were performed. In the first measurements, a virtual uniform circular array (UCA) was realized by mounting a Biconical antenna on a positioning turntable. We obtained $P = 720$ elements of the UCA array by automatically repositioning the Biconical antenna at uniform angles around a circle perimeter with $r = 0.5$ m, as shown in Fig. 2 (left). At each element position, a frequency sweep was performed for the frequency band 28–30 GHz. $N = 750$ samples were set for the frequency band. In the second measurement series, a horn antenna was mounted on the rotation center of the turntable, as shown in Fig. 2 (right). To make meaningful comparison, the same measurement settings as in the first measurement series (i.e. the same frequency sweep and orientation sweep) were adopted for the second measurement series. To avoid excessive loss and phase instability

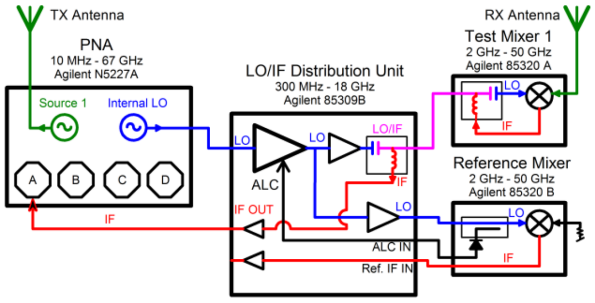

Figure 1. Block diagram of the VNA based channel sounding system. Green, blue and red denote the RF, LO and IF frequency, respectively.

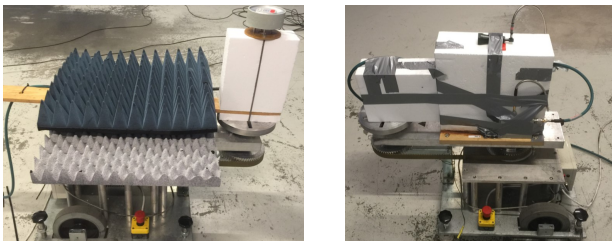

Figure 2. A photo of the Biconical antenna placement (left) and horn antenna placement (right) at the Rx.

on the cable, the signal is down-converted via using a reference mixer. Calibration was performed up to the antennas to eliminate the effects of Tx-Rx chain. The Biconical antenna at $28-30$ GHz has a gain around 5.5 dB, with a narrow beamwidth around 15^o half power beamwidth (HPBW) in the E-plane and an omnidirectional pattern in the H-plane (as shown in Fig. 3 (left)). The horn antenna at 28 - 30 GHz has around 21^o HPBW both in the H-plane and E plane, with a gain of 18.5 dBi, as shown in Fig. 3 (right). Note that Tx and Rx were placed at the same height for both measurement scenarios.

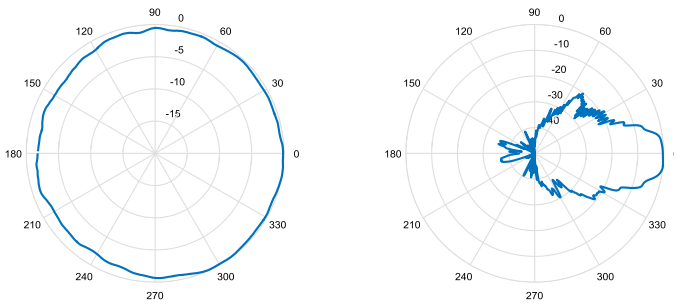

Figure 3. Measured radiation pattern of Biconical antenna (left) and horn antenna (right) in the H-plane. The measured antenna pattern of the Biconical is quasi-omnidirectional, with a maximum deviation of 2.1 dB.

Figure 4. A photo of the LOS scenario (Biconical antenna as the Rx antenna) and the obstructed LOS scenario (Horn antenna as the Rx antenna).

2.2 Measurement scenario

The measurments were performed in an empty basement, which is a $7.7 \times 9.1 \times 3.3$ m^3 room with an open corridor, as depicted in Fig. 4. Both the line-of-sight (LOS) scenario and obstructed obstructed-LOS scenarios were measured. A total of four measurement campaigns were performed, i.e. two measurement scenarios and two types of Rx antennas for each scenario.

3 Channel Estimation Algorithms

3.1 Rotational directive antenna

Channel sounding with a rotational horn is straightforward and widely utilized in the literature for the mm-Wave band sounding purposes. Basically, we can measure one impulse response for each antenna orientation. Via rotating the horn antenna in different angles, we can obtain the spatial profile of the channel directly. The downside of the rotational horn measurement is the mechanical steering and wide beamwidth inherent with the directive antenna.

The measured power-angle-delay profiles with the rotational horn at the Rx side can be directly obtained, via performing inverse Fourier transform of the recorded channel frequency responses for each rotation. For the LOS scenario, as we can see in Fig. 5, the LOS path is dominant and only a few specular paths due to LOS propagation and specular reflections were identified. The measured results with rotational horn antenna suffers from low spatial resolution, as expected. The measured result for the obstructed LOS scenario is shown in Fig. 6. Multipath components identified in the LOS and O-LOS scenarios are quite similar, except the paths impinging the Rx with AoAs around 0^o and 180^o, which are blocked by the blackboard.

3.2 Virtual UCA

Different channel estimation algorithms can be applied to extract the radio channel parameters based on the received frequency response at each virtual array element (i.e. antenna locations). Below three channel estimation algorithms for the virtual UCA are briefly explained.

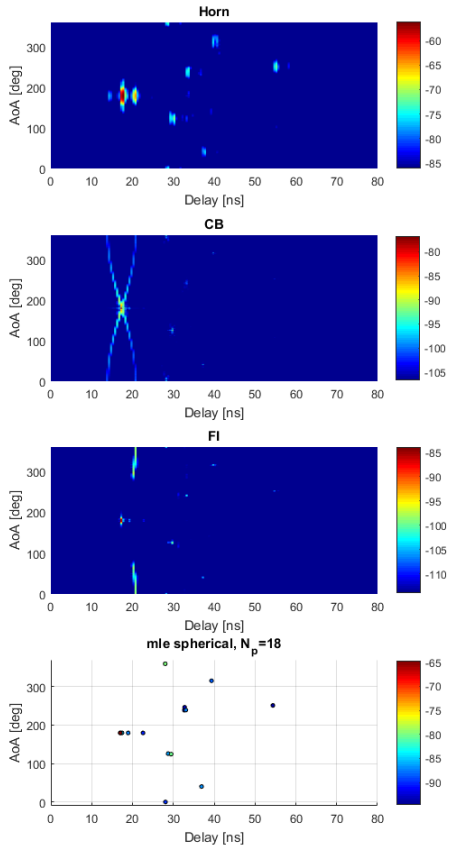

Figure 5. LOS

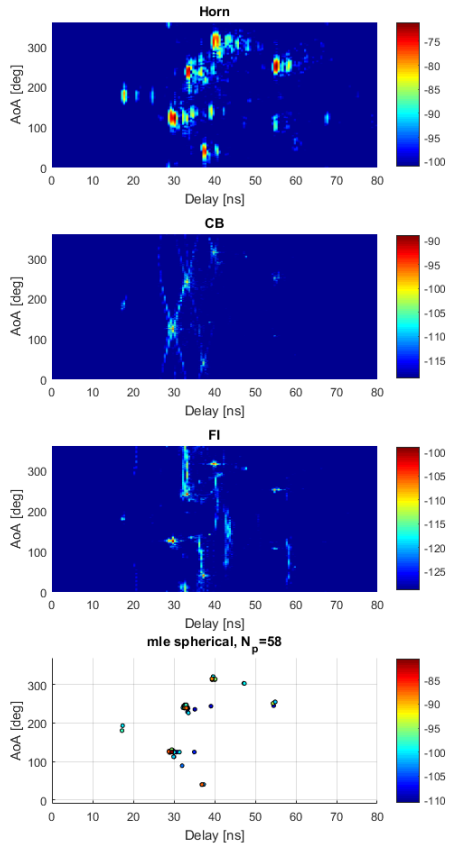

Figure 6. NLOS

3.2.1 Classical beamforming (CB)

The basic idea of the classical beamformer is that we can set the array element phase weight such that signals add up constructively at the target directions [4]. The measured power-angle-delay profiles with the UCA, although with higher spatial resolution for the mean beam, suffers from high side lobes as well. As explained in [4], the joint sidelobes in delay and angle domains are caused by the joint frequency and angle dependence with the conventional beamforming technique. The conventional beamformer for UCA is frequency variant, which in turn generates joint high sidelobes in delay and angle domains. As we can see in Fig. 5 and Fig. 6, the same paths are identified with the CB and rotational horn antenna measurement. The measured results demonstrate that the CB algorithm works as expected. The measured results with the CB algorithm suffer from joint sidelobes in angle and delay domain.

3.2.2 Frequency invariant beamforming (FI)

The basic idea of FI is that we can achieve approximately invariant beam patterns over broad frequency bands and constant beam patterns over the UCA plane. It can be utilized for wideband joint angle-of-arrival and delay-of-arrival estimation [6]. The main problem with the FI algorithm is that sidelobes around $\varphi_k \pm \pi$ exist for every multipath componentφ_k ($k \in [1, K]$). The measured results with the FIB algorithm for the LOS and obstructed LOS scenarios are shown in Fig. 5 and Fig. 6, respectively. Excellent resolutions in delay and angle domains can be achieved, though the result suffers from the sidelobe of the LOS path.

3.2.3 Maximum likelihood estimation (MLE) algorithm

A wideband spherical-wave MLE algorithm for large-scale array systems was presented in [7]. A two-stage procedure was introduced to decrease the computational complexity significantly, which includes an initialization stage and an estimation refinement stage. Fig. 5 and Fig. 6 showed the power-angle-delay profile for both the LOS and the OLOS scenario in comparison to that measured with the other methods, respectively. For both scenarios, it can be observed that the power-angle-delay profile obtained with the MLE algorithm and the horn measurement match very well.

4 Measured Channel Characteristics

To assess the delay profiles, mean delay $\bar{\tau}$ and root mean square (RMS) delay spread σ_τ can be computed from the measured CIRs. The circular mean azimuth angle $\bar{\phi}$ and circular azimuth angle spread σ_ϕ can be calculated based on the estimated power-angle-delay profiles from the virtual UCA with different channel estimation algorithms and the rotational horn.

4.1 LOS Scenario

The calculated channel characteristics in the LOS scenario are shown in Table 1. The obtained $\overline{\phi}$ and $\overline{\tau}$ are quite similar with the rotational horn antenna measurements and the virtual array measurements with different algorithms. This is due to the fact that LOS path is dominant in the propagation scenario. Significant differences can be observed in terms of angle spread and delay spread for different channel estimation algorithms. The second order statistics of the CB and FI deviates from the rotational horn and MLE algorithm, mainly due to the high side-lobes present in the measured power-angle-delay-profiles.

Table 1. channel charateristics in the LOS scenario.

Method	$\overline{\phi}$ [^{o}]	σ_ϕ [^{o}]	$\overline{\tau}$ [^{o}]	σ_τ [^{o}]
Horn	179.3	23.9	19.2	6.2
CB	179.3	55.1	17.6	3.2
FI	182.9	94.6	19.0	3.7
MLE	178.6	24.9	18.1	3.8

4.2 NLOS

The calculated channel characteristics in the obstructed-LOS scenario are shown in Table 2. Significant differences can be observed in the channel characteristics in different channel estimation algorithms. The measured results demonstrated the impact of channel estimation algorithms in radio channel parameters.

Table 2. channel charateristics in the NLOS scenario.

Method	$\overline{\phi}$ [^{o}]	σ_ϕ [^{o}]	$\overline{\tau}$ [^{o}]	σ_τ [^{o}]
Horn	223.2	93.9	39.2	10.5
CB	155.1	92.8	32.4	5.5
FI	154.0	141.2	34.4	7.2
MLE	142.1	81.3	32.4	5.6

5 Conclusion

Measured propagation channel parameters should be independent of antennas utilized in the measurement campaign and channel estimation algorithms, when the physical propagation environments are not altered. However, in practical measurement campaigns, antennas are often inherently included in the measured results and hard to deembed their effect. Further, different channel estimation algorithms were often applied to extract the channel characteristics, and channel estimation algorithms might inherently present deficiencies. However, it was demonstrated in the paper that, if antennas and channel estimation algorithms were not properly taken into consideration, significant difference can be expected for the same propagation environment.

This paper presented the measured channel characteristics in a LOS and obstructed LOS indoor scenario using different antennas (i.e. rotational horn and virtual array) and different channel estimation algorithms (i.e. classical beamforming, frequency invariant beamforming and a low-cost maximum likehood estimator) for the virtual array. It was shown that very different channel parameters might be extracted from the same propagation scenario, if different channel estimation algorithms were utilized.

Acknowledgment

Dr. Wei Fan would like to acknowledge the financial assistance from Danish council for independent research (grant number: DFF611100525).

References

[1] B. Ai, K. Guan, R. He, J. Li, G. Li, D. He, Z. Zhong, and K. M. S. Huq, "On indoor millimeter wave massive mimo channels: Measurement and simulation," *IEEE Journal on Selected Areas in Communications*, vol. 35, no. 7, pp. 1678–1690, July 2017.

[2] T. S. Rappaport, Y. Xing, G. R. MacCartney, A. F. Molisch, E. Mellios, and J. Zhang, "Overview of millimeter wave communications for fifth-generation (5g) wireless networks ;with a focus on propagation models," *IEEE Transactions on Antennas and Propagation*, vol. 65, no. 12, pp. 6213–6230, Dec 2017.

[3] R. He, B. Ai, G. L. Stuber, G. Wang, and D. Z. Zhong, "Geometrical based modeling for millimeter wave mimo mobile-to-mobile channels," *IEEE Transactions on Vehicular Technology*, vol. PP, no. 99, pp. 1–1, 2017.

[4] W. Fan, I. Carton, J. Ø. Nielsen, K. Olesen, and G. F. Pedersen, "Measured wideband characteristics of indoor channels at centimetric and millimetric bands," *EURASIP Journal on Wireless Communications and Networking*, vol. 2016, no. 1, p. 58, 2016.

[5] C. Gentile, A. J. Braga, and A. Kik, "A comprehensive evaluation of joint range and angle estimation in ultra-wideband location systems for indoors," in *2008 IEEE International Conference on Communications*, May 2008, pp. 4219–4225.

[6] F. Zhang, W. Fan, and G. F. Pedersen, "Frequency invariant uniform circular array for wideband mm-wave channel characterization," *IEEE Antennas and Wireless Propagation Letters*, 2016.

[7] Y. Ji, W. Fan, and G. F. Pedersen, "Channel estimation using spherical-wave model for indoor los and obstructed los scenarios," in *2017 11th European Conference on Antennas and Propagation (eucap)*, 2017.